

Structural, Electronic and Charge Transfer Studies of Highly Sensitive Fluorescent Probe 2-((*E*)-2-(1-phenyl-1H-phenanthro[9,10-d]imidazol-2-yl)vinyl)phenol: Quantum Chemical Investigations

V. Thanikachalam · J. Jayabharathi · A. Arunpandiyan · P. Ramanathan

Received: 4 August 2013 / Accepted: 11 September 2013 / Published online: 6 October 2013
© Springer Science+Business Media New York 2013

Abstract This article presents a facile synthesis of novel class of bluish-green fluorescent 2-((*E*)-2-(1-phenyl-1H-phenanthro[9,10-d]imidazol-2-yl)vinyl)phenol [PPIVP] and their optical, electrochemical and thermal properties. Detailed photophysical and quantum chemical studies have been performed to elucidate the origin of the dual emission shifts. PPIVP undergo excited state intramolecular proton transfer (ESIPT) reaction leading a large Stoke's shifted fluorescence emission from the phototautomer. The results of quantum chemical investigations not only confirmed the intramolecular charge transfer characteristics of the ESIPT tautomers but also provided a rationale for the observed high fluorescence quantum efficiency in the solid state. The high photoluminescence quantum yield in the solid state is ascribed to twisted chromophores due to phenyl substituents at 1,2-position of the phenanthroimidazole ring which restricted intramolecular motion, leading to an optically allowed lowest optical transition without self quenching.

Keywords PEC · NBO · ESIPT · HOMO-LUMO · ICT

Introduction

Proton- and charge-transfer reactions are most fundamental processes involved in chemical reactions as well as in living systems [1–3]. Among the various studies of proton transfer,

organic molecules exhibiting excited-state intramolecular proton transfer (ESIPT) have attracted considerable research interest due to their optoelectronic applications such as UV photostabilizers [4], photoswitches [5], fluorescent probes [6, 7], and organic light-emitting diodes (OLEDs) [8, 9]. Hydroxyphenylbenzazole derivatives exhibit ESIPT [10–18] and are used as fluorescent probes [19] (for the labelling of proteins and DNA) and model base pairs [20] (for studying the environments within the major and minor grooves of DNA duplexes).

The ESIPT molecules exhibit low fluorescence quantum efficiency in the solid state is due to concentration quenching. Aiming at the high performance OLEDs as well as the solid-state lasers, a high value of solid-state fluorescence quantum efficiency is in demand to contribute to the improvement of their technological applications [21, 22]. Conjugated organic small molecules that showed high quantum yield in the solid state without concentration quenching problem [23–29]. In solution, the conjugated backbone of these molecules is significantly twisted by steric hindrance [24] and the radiative decay pathway of the resulting twisted chromophores [25] is generally suppressed as they dissipate energy for molecular rotation. In the solid state, the twisted conjugated backbone enhances the emissive property of the molecules because the molecular rotation is hindered by adjacent molecules upon aggregation [24–29].

In the present article, we report our precise investigation on ESIPT, based on the spectral and photophysical properties of newly synthesized 2-((*E*)-2-(1-phenyl-1H-phenanthro[9,10-d]imidazol-2-yl)vinyl)phenol [PPIVP]. Steady state absorption and emission techniques are exploited for the purpose. The spectroscopic observations have been correlated with the theoretical results. Density functional theory (DFT) and time

V. Thanikachalam (✉) · J. Jayabharathi · A. Arunpandiyan · P. Ramanathan
Department of Chemistry, Annamalai University,
Annamalainagar 608 002, Tamilnadu, India
e-mail: vtchalam2005@yahoo.com

dependent density functional theory (TDDFT) are used to simulate the ground state and the excited state potential energy curves (PECs) respectively. The simulated PECs, Mulliken charge and natural bond orbital (NBO) analysis reveal that the intramolecular proton transfer reaction is feasible in the excited S_1 state but not in the ground state S_0 .

Experimental

Spectral Measurements

The proton spectrum at 400 MHz was obtained at room temperature using a Bruker 400 MHz NMR spectrometer. Proton decoupled ^{13}C NMR spectrum was also recorded at room temperature employing a Bruker 400 MHz NMR spectrometer operating at 100 MHz. The mass spectrum of the sample was obtained using a Thermo Fischer LC-Mass spectrometer in fast atom bombardment (FAB) mode. The UV–vis absorption and fluorescence spectra were recorded with PerkinElmer Lambda 35 spectrophotometer and PerkinElmer LS55 spectrofluorimeter, respectively.

$$\beta_{\text{tot}} = \left(\beta_x^2 + \beta_y^2 + \beta_z^2 \right)^{1/2} \quad (or) \quad (3)$$

$$\beta_{\text{tot}} = \left[(\beta_{xxx} + \beta_{xyy} + \beta_{xzz})^2 + (\beta_{yyy} + \beta_{yzz} + \beta_{yxx})^2 + (\beta_{zzz} + \beta_{zxx} + \beta_{zyy})^2 \right]^{1/2}$$

The β components of Gaussian output are reported in atomic units and therefore the calculated values are converted into e.s.u. units (1 a.u. = 8.3693×10^{-33} e.s.u.).

Natural Bond Orbital (NBO) Analysis

The second order Fock matrix was carried out to evaluate the donor-acceptor interactions in PPIVP by NBO analysis [32]. For each donor (i) and acceptor (j), the stabilization energy $E(2)$ associated with the delocalization $i \rightarrow j$ is estimated as,

$$E(2) = \Delta E_{ij} = q_i \frac{F(i, j)^2}{\epsilon_j - \epsilon_i} \quad (4)$$

Where q_i is the donor orbital occupancy, ϵ_i and ϵ_j are diagonal elements and $F(i, j)$ is the off diagonal NBO Fock matrix element. The larger the $E(2)$ value, the more intensive is the interaction between electron donors and electron acceptors.

Computational Details

The quantum chemical calculations were performed using the Gaussian-03 [30] package. Computations of the vertical excitations, difference density plots and optimization of the ground and excited states were performed using density functional theory (DFT) and time-dependent DFT (TD-DFT) using B3LYP/6-31G (d,p) basis set, respectively. The ground and excited states HOMO and LUMO frontier orbitals of PPIVP were calculated by both DFT and TD-DFT methods at the B3LYP/6-31G(d,p) level.

Hyperpolarizability

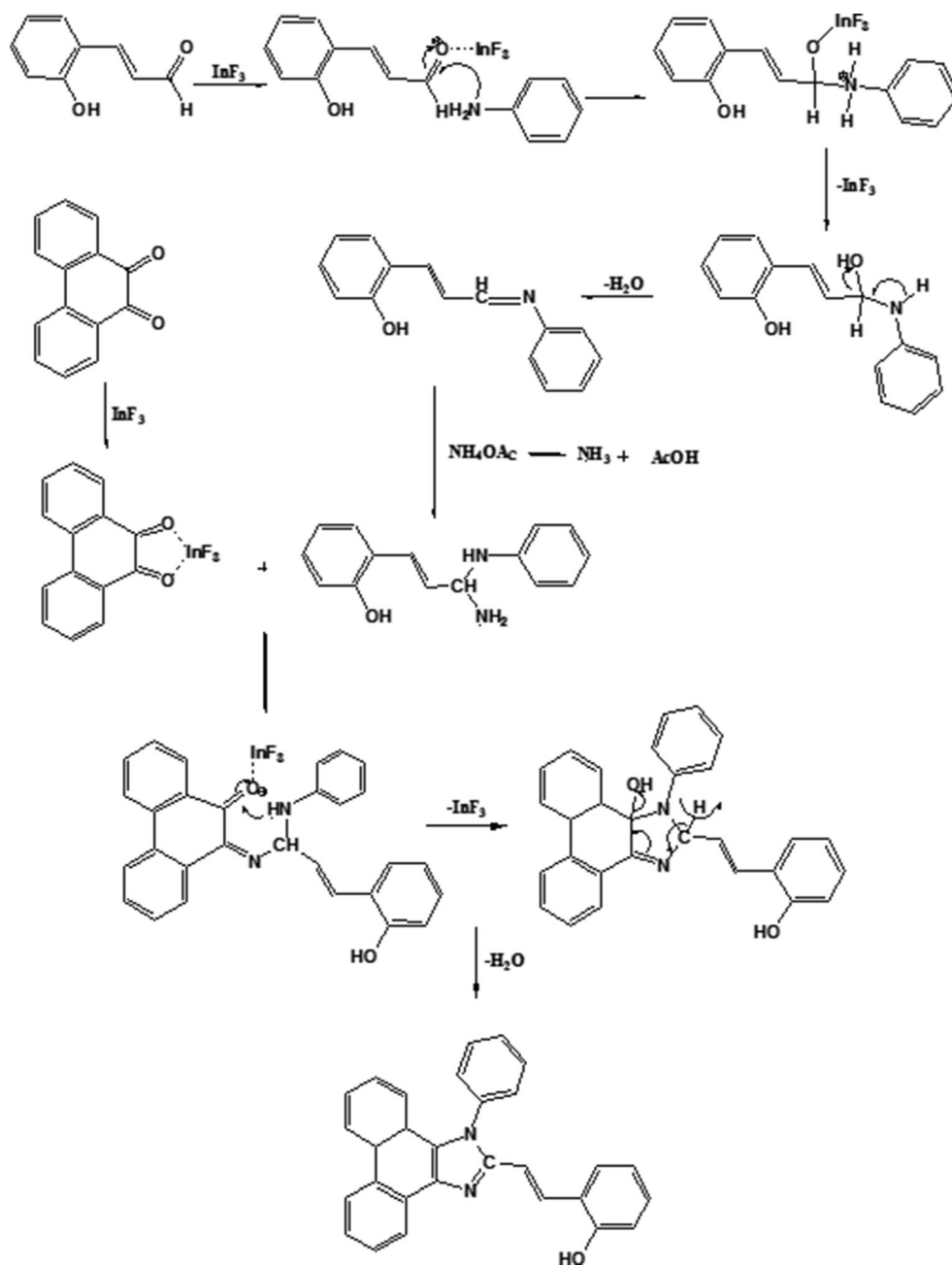
The density functional theory has been used to calculate the dipole moment (μ), mean polarizability (α) and the total first static hyperpolarizability (β) [31] for PPIVP in terms of x, y, z components and is given by following equations.

$$\mu = \left(\mu_x^2 + \mu_y^2 + \mu_z^2 \right)^{1/2} \quad (1)$$

$$\alpha = 1/3(\alpha_{xx} + \alpha_{yy} + \alpha_{zz}) \quad (2)$$

Synthesis of 2-phenylimidazol-2-yl)-2-(1-phenyl-1H-phenanthro[9,10-d]imidazol-2-yl)vinyl phenol (PPVIP) by InF_3

A mixture of 2-hydroxycinnamaldehyde (1 mmol), phenanthroquinone (1 mmol), aniline (1 mmol), ammonium acetate (1 mmol) and indium trifluoride (InF_3) (1 mol %) were stirred at 80 °C. The progress of the reaction was monitored by TLC (Scheme 1). After completion of the reaction, the mixture was cooled, dissolved in acetone and filtered. The product was purified by column chromatography using benzene: ethyl acetate (9:1) as the eluent. M.p. 200 °C., Anal. calcd. for $\text{C}_{29}\text{H}_{20}\text{N}_2\text{O}$: C, 84.44; H, 4.89; N, 6.79; O, 3.88. Found: C, 84.42; H, 4.87; N, 6.77; O, 3.86. ^1H NMR (400 MHz, DMSO): δ , 13.99 (s, 1H), 6.69 (d, $J=16\text{Hz}$, 1H), 7.07 (d, $J=7.6\text{Hz}$, 1H), 7.361–7.333 (m, 6H), 7.537–7.479 (m, 3H), 7.682–7.870 (m, 8H), 8.21 (d, $J=7.6\text{Hz}$, 1H), 8.87 (q, $J=8.0\text{Hz}$, 2H), ^{13}C NMR (100 MHz, DMSO): δ 113.82, 120.17, 122.12, 123.65, 124.46, 125.21, 125.81, 126.46, 126.66, 126.84, 127.22, 127.42, 127.79, 128.29, 128.32, 128.66, 128.79, 128.92, 130.38, 130.53, 134.38, 135.69, 136.73, 136.93, 149.24. MS: m/z. 412[M⁺].

Scheme 1 Possible mechanism for catalytic synthesis of PPIVP

Results and Discussion

ESIPT Process

The fluorescence spectra of PPIVP in dioxane display a dual emission, observed at 361.78 nm and another in bluish-green region at 419.99 nm (Fig. 1). This dual emission of PPIVP is explained as follows: the most stable form of the ESIPT molecules in the ground state is in equilibrium between several different conformers (Fig. 2) arising from tautomerism and rotamerism [10]. The normal planar *syn* form (N_{syn}) features an intramolecular hydrogen bond between acidic

hydroxyl group and the basic nitrogen atom of the imidazole ring. The N_{syn} conformer can undergo proton transfer to form its tautomer (T_{syn}). Upon excitation of the normal form to its first excited singlet state (N_{syn}^*), undergoes an excited state intramolecular proton transfer to yield the planer tautomer T_{syn}^* accompanied with large Stokes' shifted fluorescence emission (419.99 nm). The *syn*-conformers can rotamerize to form their non-planar anti forms (N_{anti} and T_{anti} , respectively). In a protic solvent, the N_{anti} conformer can form intermolecular hydrogen bonds with solvent molecules (Fig. 2, I) but it cannot undergo ESIPT. Therefore, dual emission is observed in non-polar solvents. In addition to the fluorescence from the T

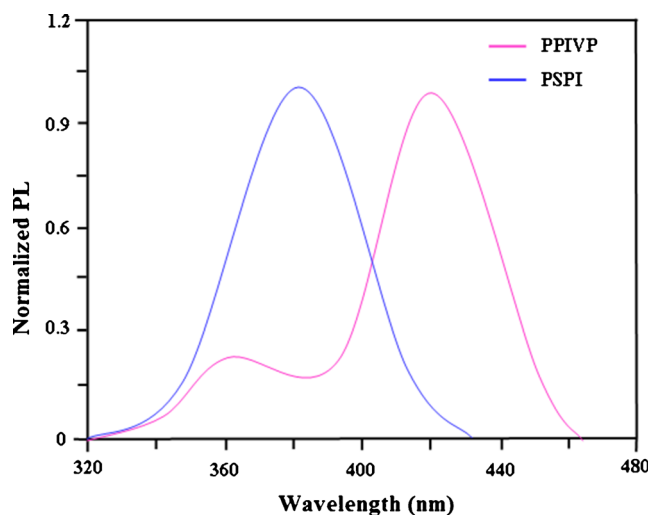


Fig. 1 Competition of intramolecular hydrogen bonding of the PPIVP and PSPI

N_{syn}^* form, the N_{anti}^* form can also exhibit normal Stokes' shifted weak fluorescence at 361.78 nm [18, 33]. Moreover, the typical ESIPT process produces the tautomeric form can be coupled with the intramolecular charge transfer (ICT) state with a rotation around interannular bond to produce a non-planar

Fig. 2 Structures of various isomers of PPIVP in the ESIPT and ICT processes

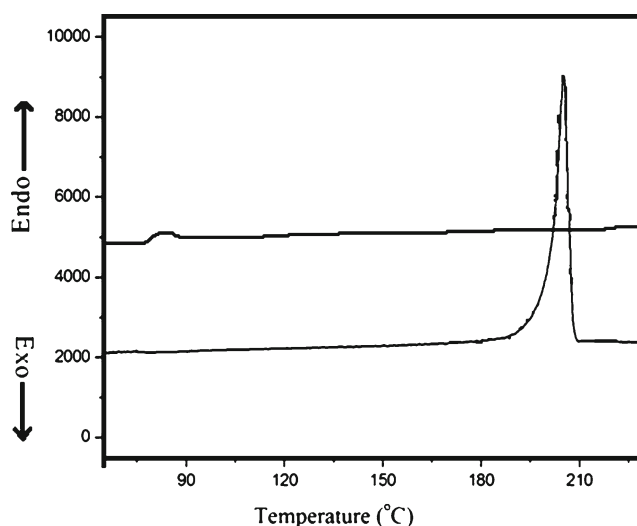
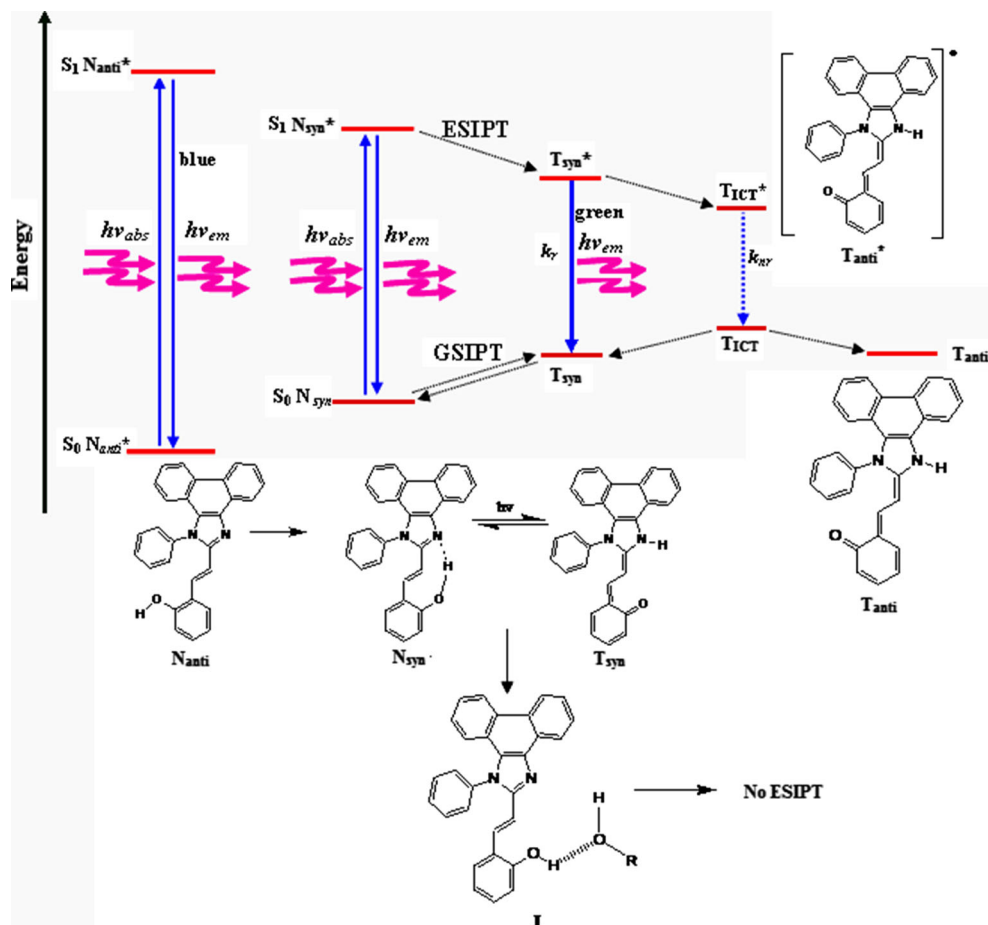
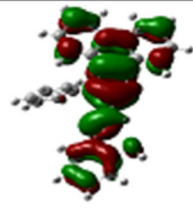
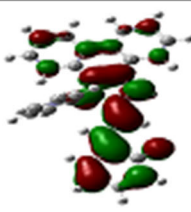
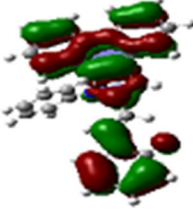
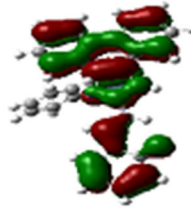
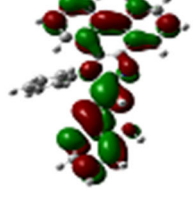
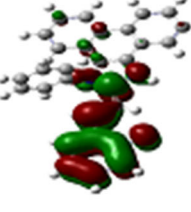
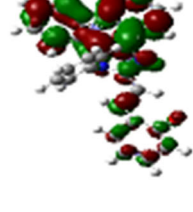
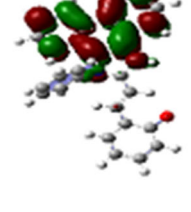


Fig. 3 Differential scanning calorimetry of PPIVP

configuration (T_{ICT}^*) between the two rings. The T_{ICT}^* state can be deactivated back to its ground state via radiationless relaxation.

The existence of intramolecular hydrogen bond in PPIVP is confirmed by the presence of the singlet at 13.99 ppm in the 1H NMR spectrum which is a typical signal for hydrogen

Fig. 4 HOMO – LUMO surface diagram in N_{syn} and N_{anti} form of PPIVP

Form	ENOL	KETO
HOMO	 -5.31 (eV)	 -4.82 (eV)
HOMO-1	 -5.48 (eV)	 -5.28 (eV)
LUMO	 -2.05 (eV)	 5.61 (eV)
LUMO+1	 -3.61 (eV)	 5.81 (eV)

bonded hydrogen atom. The parent compound 1-phenyl-2-styryl-1H-phenanthro[9,10-d]imidazole (PSPI) exhibits emission peak only at 382 nm. Absence of additional peak at longer wavelength confirms absence of intramolecular hydrogen bond in parent compound (Fig. 1). It is further evident that intramolecular hydrogen bonding is the driving force for ESIPT and the dual fluorescence emission.

Quantum Chemical Calculations and Photophysical Properties

Owing to their rigid and non-coplanar structures, PPIVP is expected to decrease the intermolecular stacking efficiency

due the steric crowding. Therefore, it is expected to exhibit good solubility without loss of their excellent thermal properties. The diaryl substituted phenanthrimidazoles PPIVP exhibited high melting point (T_m) around 200 °C. In addition, distinct glass transition temperature (T_g) could be observed at 78.3 °C (Fig. 3). The observed T_g and T_m values suggest that the PPIVP has amorphous nature in condensed state, which may greatly benefit the formation of homogeneous and amorphous films through thermal evaporation.

PPIVP exhibits the absorption peaks around 318, 262, 311 and 345 nm (10^{-4} M) in chloroform, acetonitrile, 1-propanol and methanol at room temperature, which can be considered to be absorptions belonging to π - π^* transitions on the basis of

extinction coefficients and oscillator strengths (f) from molecular orbital (MOs) calculation. The molar absorption coefficients range between 12,500 and 38,100 $\text{cm}^{-1} \text{M}^{-1}$, is the typical range for allowed π - π^* transitions. The distinct vibrational structured, spectra of 2-phenyl-9,10-phenanthroimidazole (PhI) [34] is due to the conjugation of the π system extended by the electronic substituents on the 1,2 positions of the imidazole ring leading to the prominence of a π - π^* nature of transition to the excited states rather than n - π^* . In the solid thin films, the chromophores maintained similar absorption spectral positions to those of the solution. The optical bandgap (E_g) of PPIVP is lower than PhI ($E_g=3.522$ eV in CH_3CN) [35] because of the lower HOMO energy level as shown in Fig. 4. This may be due to the presence of charge transporting substituents on the phenanthroimidazole moiety.

The solid state fluorescence quantum efficiency of PPIVP is 0.63 whereas the same in solution is 0.51. PPIVP displayed a very brilliant solid film photoluminescence in the bluish-green region of the visible spectrum at room temperature. Besides electronic effect, there is probably an interesting steric effect of the multiple phenyl substituents on molecular arrangements in solid state, and is most probably interacts in an offset face-to-face fashion with another imidazolyl ring of a contiguous moiety in PPIVP. Possibly, the relative small intermolecular π - π overlapping areas of these diaryl phenanthrimidazoles compared with that of mono-aryl phenanthrimidazoles is probably a key factor that accounts for their high fluorescence quantum yield in the solid state and in the thin film. The corresponding intramolecular motions and relative free rotation of end phenyl groups in solution may be the origin of weak fluorescence. In the solid state, the free-rotation occurring in solution will be depressed due to the intermolecular interaction, which is beneficial to enhanced fluorescent efficiency the substituents in the ESIPT molecules that favour the ICT from the proton donor to the proton acceptor moiety will increase the nonradiative decay and, consequently, decrease the fluorescence quantum yield.

To study further about the relationship between their molecular structures and optical properties, the geometrical parameters of $N_{\text{syn}}-T_{\text{syn}}$ tautomers and their energy-minimized, preferred conformations were calculated by DFT using B3LYP/6-31G(d,p) [36]. The geometry optimization in the S_0 and S_1 of N_{syn} , T_{syn} and transition state (TS) of the phenanthrimidazoles was performed and respective parameters are listed in Table 1. As shown in Table 1, in the S_0 and S_1 for N_{syn} form, the distance of $N_{17}\cdots H_{52}$ in PPIVP was about 1.66 Å. It is well known that H-bond is short distance force in essence; hence the H-bond force between H and N should be operating in the N_{syn} form. On the other hand, the distance of $N_{17}\cdots H_{52}$ was too short (1.03 Å) in the S_0 and S_1 for the T_{syn} form. Generally, the $N_{\text{syn}} \rightarrow T_{\text{syn}}$ tautomerization brought a variation of the chemical bond length of phenolic ring. The maximum of the difference between the bond lengths of phenolic $O_{51}-H_{52}$ in the N_{syn} form of PPIVP is 0.96 Å, while

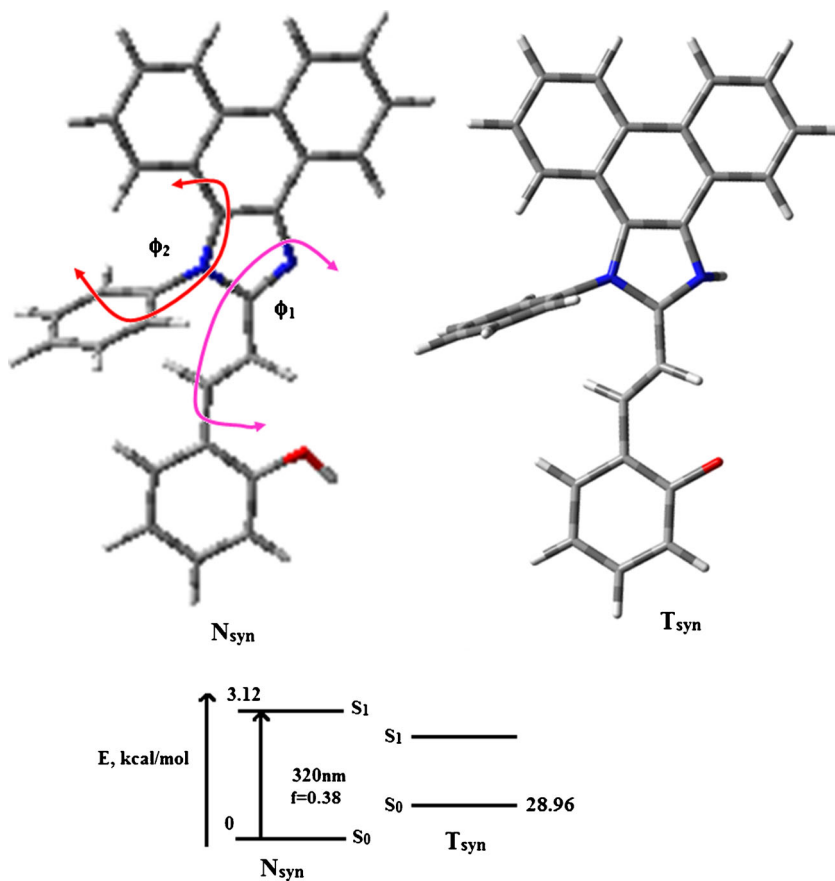
Table 1 Selected optimized geometry parameters for the enol and keto-forms of PPIVP

Geometry parameters	enol (N_{syn})	Keto (T_{syn})
Relative energy/kcal $\text{mol}^{-1} S_0(S_1)$	0.00(3.12)	28.96(0.00)
Dipole moment (μ)D	4.41	7.06
Bond length (Å)		
$O_{51}-H_{52}$	0.96	1.45
$N_{17}\cdots H_{52}$	2.66	–
$N_{17}-C_{16}$	1.35	1.43
$O_{51}-C_{43}$	1.38	1.25
$N_{17}-C_{10}$	1.39	1.42
$N_{17}-H_{52}$	–	1.03
$N_{17}\cdots H_{52}$	1.66	–
$C_{39}-C_{37}$	1.34	1.42
$C_{16}-C_{35}$ (interannular bond length)	1.46	1.37
$C_{41}-C_{30}$	1.45	1.37
$C_{43}-C_{41}$	1.41	1.47
$C_{40}-C_{38}$	1.46	1.32
Bond angle ($^\circ$)		
$\langle H_{52}-O_{51}-C_{43}$	108.15	–
$\langle N_{17}-C_{16}-C_{31}$	123.66	125.29
$\langle C_{37}-C_{39}-C_{41}$	126.08	126.57
$\langle C_{41}-C_{43}-O_{51}$	108.17	124.43
$\langle O_{51}-C_{43}-C_{41}$	–	123.54
$\langle N_{17}-C_{16}-H_{52}$	–	118.81
Dihedral angle ($^\circ$)		
$\langle C_{10}-N_{17}-C_{16}-C_{37}$	83.9 $^\circ$	88.2 $^\circ$
$\langle N_{17}-H_{52}-C_{16}-C_{36}$	13.2 $^\circ$	3.1 $^\circ$
Excitation energy/nm	320	410
Oscillator strength (f)	0.38	0.16

the value in the T_{syn} form increased to 1.45 Å, implying that aromaticity of this ring in the T_{syn} form was lost because of the internal proton transfer (ESIPT) process. Again the stable ground state geometry of N_{syn} of PPIVP had twisted bond ϕ_2 ($2'$ -ph) by 13.2 $^\circ$. Dihedral angle was decreased to 3.1 $^\circ$ during $N_{\text{syn}} \rightarrow T_{\text{syn}}$ tautomerization, reflecting that the extent of molecular distortion was reduced Fig. 5. In a system with a great delocalization of π -electron, the torsion angle decided whether the molecule could be well-conjugated. Consequently, the small twisted configuration in the excited state allowed the extension of the conjugated π -electron in the entire molecular framework and the energy barrier in the ESIPT process caused by the ground state twisting was reduced. It was favourable to undergo ESIPT for PPIVP.

The plots of the potential curves of internal proton transfer in S_0 and S_1 states of PPIVP as a function of $O_{51}-H_{52}$ distance were performed and presented in Fig. 6, which shows clearly that the N_{syn} form is most stable in the S_0 state whereas the T_{syn} form is most stable in the S_1 state. ΔE (energy difference between N_{syn} and T_{syn}) again reveals that T_{syn} form has a

Fig. 5 Molecular modelling of PPIVP using Gaussian-03



higher energy than N_{syn} form in S_0 state as the aromatic ring is broken by proton transfer. The activation barrier for $N_{syn} \rightarrow T_{syn}$ in S_0 electronic state is $28.96 \text{ kcal mol}^{-1}$, large enough to make the ground state intramolecular proton transfer (GSIPT) unviable under thermal conditions, whereas upon photoexcitation, much smaller interconversion barrier ($N_{syn}^* \rightarrow T_{syn}^*$) of $3.12 \text{ kcal mol}^{-1}$ in S_1 state preferably allows ESIPT to give

the large Stokes' shifted fluorescence emission. After decaying to the ground state, the phototautomer T_{syn}^* reverts to the original N_{syn} via reverse proton transfer barrier (ΔE_r^\ddagger) of $9.86 \text{ kcal mol}^{-1}$. This implied that although the occurrence of GSIPT from $N_{syn} \rightarrow T_{syn}$ should be very difficult, the reverse proton transfer process from $T_{syn} \rightarrow N_{syn}$ could take place easily, which was much favourable for ESIPT occurrence. Finally, the protons transfer from T_{syn} to the starting N_{syn} in thermal processes in S_0 states to finish the cyclic four-level photophysical scheme ($1N_{syn} \rightarrow 1N_{syn}^* \rightarrow 1T_{syn}^* \rightarrow 1T_{syn} \rightarrow 1N_{syn}$), immediately after photoexcitation of the intramolecular H-bonded molecules. Therefore, an abnormally large Stokes shift without self-absorption is detected, providing an ideal scheme for UV-photostabilizers or proton transfer lasers.

The electron distribution of the frontier orbitals reflects the electron transition characteristics Fig. 4. The HOMO and

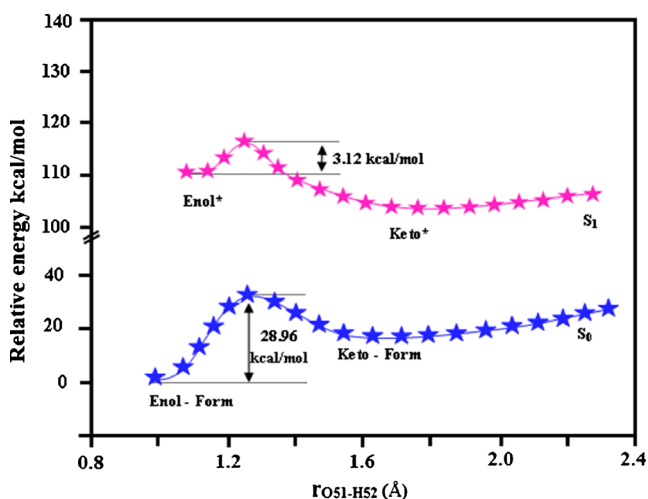


Fig. 6 Ground (S_0) and excited-state (S_1) potential energy curves (PEC) of PPIVP

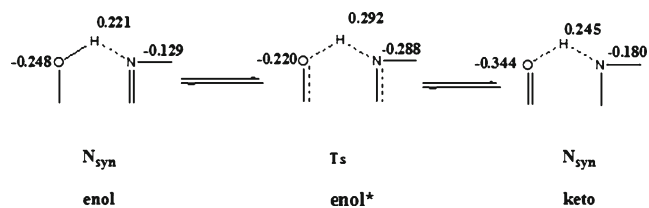
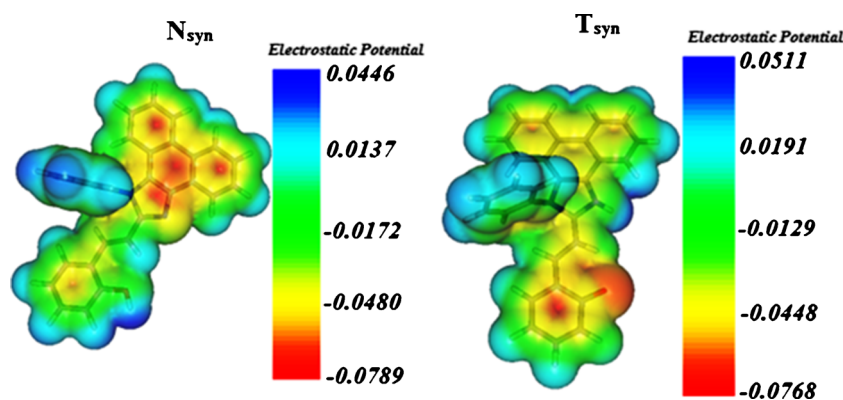


Fig. 7 Mulliken atomic charge population of ESIPT site of PPIVP

Fig. 8 MEP surface diagram of PPIVP



LUMO of substituted phenanthrimidazoles exhibited π -type symmetry. From HOMO to LUMO, the electron density distribution displayed the transfer from phenolic ring to phenanthrimidazole moiety. The calculated long wavelength absorption peak of PPIVP (320 nm, oscillator strength (f)=0.38) is due to a mixture of different transitions, e.g., HOMO \rightarrow LUMO, HOMO \rightarrow LUMO+1, HOMO \rightarrow LUMO+2, etc. The LUMO electron density is delocalized through the acceptor and π -bridges. This change in the electron density acts as a driving force for the very fast intramolecular proton transfer in these compounds upon excitation to the S1 state. Thus, the phenolic ring had smaller electron density in the excited state, which was driving force for the occurrence of proton transfer for PPIVP in the excited state. Hence, the HOMO \rightarrow LUMO transition could be ascribed to π - π^* excitation with internal charge transfer character [37].

The Mulliken atomic charge population of the key atoms (O_{51} - H_{52} and N_{17} - H_{52}) of HPPHl and PPIVP are shown in Fig. 7. Remarkably, as per expectation, hydrogen atom had high positive charge, which indicated that it was a real proton transfer if ES IPT or GS IPT took place. Interestingly, the positive charge of hydrogen experienced increasing and then decreasing during intramolecular proton transfer both in ground and excited states, reaching the maximum at transition state because of

largest hydrogen-bond strength. While N_{syn} was excited to N_{syn}^* , the part of negative charge was transferred from the hydroxyl to the imino group, which resulted in the change of the force balance of hydrogen bond. Consequently the negative charge of the proton donor decreased (more acidic), and the negative charge of the proton acceptor increased (more basic), which enhanced the change of geometry in the excited state and prompted the ES IPT occurrence for photoreactive hydrogen bonded chromophore. The ground-state dipole moment of the keto-form is remarkably higher (7.06D) than that of the enol-form (4.41D). Such enlargement of dipole moment for the keto-geometry provided us the impetus to extend the calculations further so as to be able to delineate the influence of solvent reaction field on the relative stabilities of various conformers, and optimized geometry parameters. The dipole moments centralized on the Y-dimension and the electronic transition led to the changes in the charge distribution, which was accompanied by the increase of the molecular dipole moments in the excited state.

MEP surface diagram (Fig. 8) is further schematic DFT evidence for the electron densities of the atoms. The negative regions can be regarded as nucleophilic centres, whereas the positive regions are potential electrophilic sites. The MEP map of PPIVP clearly suggests that the nitrogen and oxygen atoms represent the most negative potential region. The hydrogen atoms bear the maximum brunt of positive charge. The predominance of green region in the MEP surfaces corresponds to a potential halfway between the two extremes red and dark blue colour.

Table 2 Second order perturbation energies of some prominent interactions in the enol and keto-forms of PPIVP from NBO analysis

φ_i	φ_j	enol-form	keto-form
LP N_{17}	$\sigma^*C_7-C_{10}$	3.35	32.98
LP N_{17}	$\sigma^*C_9-C_{10}$	1.71	40.15
LP N_{17}	$\sigma^*N_{15}-C_{16}$	6.17	–
LP N_{17}	$\sigma^*C_{16}-C_{37}$	2.20	–
LP N_{17}	$\sigma^*O_{51}-H_{52}$	2.25	–
LP O_{51}	$\sigma^*C_{37}-H_{38}$	3.05	2.24
LP O_{51}	$\sigma^*C_{41}-C_{43}$	2.00	25.76
LP O_{51}	$\sigma^*C_{43}-C_{46}$	2.65	4.62
LP O_{51}	$\sigma^*C_{42}-C_{45}$	–	25.50

(φ_i donor NBO, φ_j acceptor NBO)

Table 3 Electric dipole moment (μ , D), polarizability (α , 10^{-30} esu) and hyperpolarizability (β_{tot} , 10^{-32} esu) of enol and keto forms of PPIVP

S.No.	Parameters	Enol	Keto
1	Dipole moment	4.41	7.06
2	Polarizability	3.27	5.33
3	Hyperpolarizability	34.47	2.13
4	r	44.83	269.49
5	$\mu\beta_0$	152.01	59.60

Restricted intramolecular/intermolecular motion [21–29] has been suggested as one of the most significant mechanisms of aggregation-induced emission enhancement phenomenon. In dilute solutions of molecular dispersed phenanthroimidazole, two end-substituted phenyl units of the molecule could rotate freely around the single bonds and the radiative decay would be effectively restricted by this kind of intramolecular torsion. While in the aggregate state, the intramolecular rotation and torsion were greatly impeded and therefore the non-radiative decay channel was effectively restricted, which in turn populated the irradiative state of the excited molecules and resulted in a great increase of fluorescence. Hence, it was easy to understand why the molecularly dispersed dilute solutions of phenanthrimidazoles were so weakly luminescent while their solid particles and aggregates were highly emissive. All these results in agreement with the proposed mechanism for the intramolecular H-bonded compounds PPIVP in dilute solution undergo an excited state charge transfer coupled proton transfer depicted in (Fig. 2). Upon excitation of N_{syn} an ESIPT process takes place to give T_{syn}^* fluorescent species, after which the excited tautomer undergoes a large-amplitude conformational change associated with a charge migration from deprotonated phenol moiety to the protonated imidazole moiety, yielding the non-fluorescent charge transfer intermediate T_{ICT}^* , which probably deactivates very fast [12]. The electronic and geometric structure of T_{ICT}^* in Fig. 2 is hypothetical, not only about the nature of the conformational change experienced by T_{syn}^* but also in relation to the charge distribution. Accordingly, the fluorescence enhancement in the solid state is due to the prevented T_{ICT} by kinetic constraint which blocks large amplitude twisting motion about the interannular C-C bond (torsion angle, ϕ_2) along the ESIPT reaction coordinate.

The results of NBO treatment on PPIVP have been briefly summarized in (Table 2), which reflects the collection of some prominent interactions found in the enol and keto-forms of PPIVP and the results for the IMHB interaction ($N_{17} \text{---} H_{52}$). The delocalization interactions are found to be especially sizeable for the π system and for the lone pairs of nitrogen and oxygen atoms. Table 2 clearly dictates that in enol-form the charge transfer interactions from the lone pairs of electron donor (N_{17}) are directed mainly to the antibonding orbitals on the remote part of the molecule. In case of the keto-form also, similar interactions are present to advocate for the IMHB interaction leading to the formation of eight-member quasicycle [38]. The hyperconjugative stabilization interaction ($\Delta E_{ij}^{(2)}$) between N_{17} lone pair and the $\sigma^*(O_{51}\text{---}H_{52})$ orbital is sharply diminished with elongation of the $N_{17} \text{---} H_{52}$ IMHB, justifying the presence of IMHB in the eight-member quasicycle. However, it is noteworthy that in spite of the reasonable sensitivity of the hyperconjugative stabilization interaction ($\Delta E_{ij}^{(2)}$) between N_{17} lone pair and the $\sigma^*(O_{51}\text{---}H_{52})$ orbital, $\Delta E_{ij}^{(2)}$ decreases from 2.25 kcal/mol in the

optimized structure ($N_{17} \text{---} H_{52}$ IMHB distance=2.66 Å) to 1.21 kcal/mol in a geometry in which the $N_{17} \text{---} H_{52}$ IMHB distance has been elongated to 2.96 Å. This suggests that the change is not as drastic as is normally observed for a strong IMHB [39], suggesting the presence of weak hydrogen bonding interaction PPIVP. This observation supports the presence of relatively weak IMHB should put its signature on the way to ascertain an ESIPT in PPIVP with a finite and well-defined barrier.

Theoretical investigation plays an important role in understanding the structure–property relationship, which is able to assist in designing novel NLO chromophores. The electrostatic first hyperpolarizability (β) and dipole moment (μ) of the imidazole chromophore have been calculated by using Gaussian 03 package [30]. From Table 3, it is found that the phenanthroimidazole chromophore show larger $\mu_g \beta_o$ value, which is attributed to the positive contribution of their conjugation. This chromophore exhibits larger non-linearity and its λ_{abs} is red-shifted when compared with unsubstituted imidazole. Therefore, it is clear that the hyperpolarizability is a strong function of the absorption maximum. Since even a small absorption at the operating wavelength of optic devices can be detrimental, it is important to make NLO chromophores as transparent as possible without compromising the molecule's non-linearity. The observed positive small ρ^{2D} value (0.14) reveals that the β_{iii} component cannot be zero and these are dipolar component. Since most of the practical applications for second order NLO chromophores are based on their dipolar components, this strategy is more appropriate for designing highly efficient NLO chromophores.

Conclusions

This article presents a facile synthesis of novel class of bluish-green fluorescent 2-((E)-2-(1-phenyl-1H-phenanthro[9,10-d]imidazol-2-yl)vinyl)phenol [PPIVP] and their optical, electrochemical, and thermal properties. The branched imidazole are more emissive than their linear 2-phenyl-1H-phenanthro[9,10-d]imidazole analogs, both in solution and when aggregated, presumably because of increased π -electron contributions to the electronic structure of the molecule, as well as restricted nonradiative deactivation resulting from less facile rotational deactivation via the interannular C-C bond (torsion angle, ϕ_2). The quantum chemical studies reveal that the formation of non-fluorescent isomers (T_{ICT}^*) of PPIVP was effectively suppressed in the solid state due to the bulky substituents (phenyl and styryl) preventing a large-amplitude conformational change in the excited-state. The ESIPT dye containing branched groups showed excellent thermal properties with high T_g (78.3 °C) and an efficient large Stokes' shifted emission with very high fluorescence quantum yield in the neat solid films without free from concentration self-quenching. The molecular design concept

established in this study should provide guidelines for fine-tuning the emission properties of this class of ESIPT fluorophore, which is beneficial for developing a new class of advanced optoelectronic applications.

Acknowledgments One of the authors Prof. J. Jayabharathi is thankful to DST [No. SR/S1/IC-73/2010], DRDO (NRB-213/MAT/10-11) and CSIR (NO 3732/NS-EMRII) for providing funds to this research study.

References

- Richard JP, Amyes TL (2001) Proton transfer at carbon. *Curr Opin Chem Biol* 5(6):626–633
- Burnworth M, Rowan SJ, Weder C (2007) Fluorescent sensors for the detection of chemical warfare agents. *Chem Eur J* 13:7828–7836
- Stoner-Ma D, Jaye AA, Ronayne KL, Nappa J, Meech SR, Tonge PJ (2008) *J Am Chem Soc* 130:1227–1235
- Paterson MJ, Robb MA, Blancafort L, DeBellis AD (2005) Mechanism of an exceptional class of photostabilizers: a seam of conical intersection parallel to excited state intramolecular proton transfer (ESIPT) in o-Hydroxyphenyl-(1,3,5)-triazine. *J Phys Chem A* 109:7527–7537
- Lim S-J, Seo J, Park SY (2006) Photochromic switching of excited-state intramolecular proton-transfer (ESIPT) fluorescence: a unique route to high-contrast memory switching and nondestructive readout. *J Am Chem Soc* 128:14542–14547
- Klymchenko AS, Shvadchak VV, Yuschenko DA, Jain N, Mély Y (2008) *J Phys Chem B* 112:12050–12055
- Ozürk T, Klymchenko AS, Capan A, Oncul S, Cikrici S, Taskiran S, Tasan B, Kaynak S, Ozbey FB, Demchenko AP (2007) *Tetrahedron* 63:10290–10299
- Sakai K-I, Tsuzuki T, Itoh Y, Ichikawa M, Taniguchi Y (2005) Using proton-transfer laser dyes for organic laser diodes. *Appl Phys Lett* 86:081103–081103
- Formosinho SJ, Arnaut LG (1993) Excited-state proton transfer reactions II. Intramolecular reactions. *J Photochem Photobiol* 75: 21–48
- Tsai H-HG, Sun H-LS, Tan C-J (2010) TD-DFT study of the excited-state potential energy surfaces of 2-(2'-Hydroxyphenyl)-benzimidazole and its amino derivatives. *J Phys Chem A* 114:4065–4079
- Vázquez SR, Rodríguez MCR, Mosquera M, Rodríguez-Prieto F (2008) *J Phys Chem A* 112:376–387
- Vázquez SR, Rodríguez MCR, Mosquera M, Rodríguez-Prieto F (2007) *J Phys Chem A* 111:1814–1826
- Yang G, Dreger ZA, Li Y, Drickamer HG (1997) Pressure-induced isomerization of 2-(2'-Hydroxyphenyl)benzoxazole in solid media. *J Phys Chem A* 101:7948–7952
- Wang H, Zhang H, Abou-Zied OK, Yu C, Romesberg FE, Glasbeek M (2003) Femtosecond fluorescence upconversion studies of excited-state proton transfer dynamics in 2-(2'-hydroxyphenyl)benzoxazole (HBO) in liquid solution and DNA. *Chem Phys Lett* 367:599–608
- Wang R, Liu D, Xu K, Li J (2009) Substituent and solvent effects on excited state intramolecular proton transfer in novel 2-(2'-hydroxyphenyl)benzothiazole derivatives. *J Photochem Photobiol* 205:61–69
- Wu Y, Lawson PV, Henary MM, Schmidt K, Bredas J-L, Fahrni CJ (2007) Excited state intramolecular proton transfer in 2-(2'-Arylsulfonamidophenyl)benzimidazole derivatives: insights into the origin of donor substituent-induced emission energy shifts. *J Phys Chem A* 111:4584–4595
- Henary MM, Wu Y, Cody J, Sumalekshmy S, Li J, Mandal S, Fahrni CJ (2007) Excited state intramolecular proton transfer in 2-(2'-Arylsulfonamidophenyl)benzimidazole derivatives: the effect of donor and acceptor substituents. *J Org Chem* 72:4784–4797
- Wu Y, Peng X, Fan J, Gao S, Tian M, Zhao J, Sun S (2007) Fluorescence sensing of anions based on inhibition of excited-state intramolecular proton transfer. *J Org Chem* 72:62–70
- Holler MG, Campo LF, Brandelli A, Stefani V (2002) Synthesis and spectroscopic characterisation of 2-(2'-hydroxyphenyl)benzazole isothiocyanates as new fluorescent probes for proteins. *J Photochem Photobiol* 149:217–225
- Dupradeau F-Y, Case DA, Yu C, Jimenez R, Romesberg FE (2005) Differential solvation and tautomer stability of a model base pair within the minor and major grooves of DNA. *J Am Chem Soc* 127: 15612–15617
- Park S, Kwon O-H, Kim S, Park S, Choi M-G, Cha M, Park SY, Jang D-J (2005) Imidazole-based excited-state intramolecular proton-transfer materials: synthesis and amplified spontaneous emission from a large single crystal. *J Am Chem Soc* 127: 10070–10074
- Park S, Kwon JE, Kim SH, Seo J, Chung K, Park S-Y, Jang D-J, Medina BM, Gierschner J, Park SY (2009) A white-light-emitting molecule: frustrated energy transfer between constituent emitting centers. *J Am Chem Soc* 131:14043–14049
- Kim S, Chang DW, Park SY, Kawai H, Nagamura T (2002) Excited-state intramolecular proton transfer in a dendritic macromolecular system: Poly(aryl ether) dendrimers with phototautomerizable quinoline core. *Macromolecules* 35:2748–2753
- Kim S, Zheng Q, He GS, Bharali DJ, Pudavar HE, Baev A, Prasad PN (2006) Aggregation-enhanced fluorescence and two-photon absorption in nanoaggregates of a 9,10-Bis[4'-(4"-Aminostyryl)styryl]anthracene derivative. *Adv Funct Mater* 16:2317–2323
- Silva GL, Ediz V, Yaron D, Armitage BA (2007) Experimental and computational investigation of unsymmetrical cyanine dyes: understanding torsionally responsive fluorogenic dyes. *J Am Chem Soc* 129:5710–5718
- Kim S, Ohulchanskyy TY, Pudavar HE, Pandey RK, Prasad PN (2007) Organically modified silica nanoparticles co-encapsulating photosensitizing drug and aggregation-enhanced two-photon absorbing fluorescent dye aggregates for two-photon photodynamic therapy. *J Am Chem Soc* 129:2669–2675
- Chen J, Xu B, Ouyang X, Tang BZ, Cao Y (2004) *J Phys Chem A* 108:7522–7526
- Li Z, Dong Y, Mi B, Tang Y, Häussler M, Tong H, Dong Y, Lam JWY, Ren Y, Sung HH-Y, Wong KS, Gao P, Williams ID, Kwok HS, Tang BZ (2005) *J Phys Chem B* 109:10061–10066
- Tong H, Hong Y, Dong Y, Ren Y, Lam JWY, Wong KS, Tang BZ (2007) *J Phys Chem B* 111:2000–2007
- Frisch MJ, Trucks GW, Schlegel HB, Scuseria GE, Robb MA, Cheeseman JR, Montgomery JA Jr, Vreven T, Kudin KN, Burant JC, Millam JM, Iyengar SS, Tomasi J, Barone V, Mennucci B, Cossi M, Scalmani G, Rega N, Petersson GA, Nakatsuji H, Hada M, Ehara M, Toyota K, Fukuda R, Hasegawa J, Ishida M, Nakajima T, Honda Y, Kitao O, Nakai H, Klene M, Li X, Knox JE, Hratchian HP, Cross JB, Bakken V, Adamo C, Jaramillo J, Gomperts R, Stratmann RE, Yazyev O, Austin AJ, Cammi R, Pomelli C, Ochterski JW, Ayala PY, Morokuma K, Voth GA, Salvador P, Dannenberg JJ, Zakrzewski VG, Dapprich S, Daniels AD, Strain MC, Farkas O, Malick DK, Rabuck AD, Raghavachari K, Foresman JB, Ortiz JV, Cui Q, Baboul AG, Clifford S, Cioslowski J, Stefanov BB, Liu G, Liashenko A, Piskorz P, Komaromi I, Martin RL, Fox DJ, Keith T, Al-Laham MA, Peng CY, Nanayakkara A, Challacombe M, Gill PMW, Johnson B, Chen W, Wong MW, Gonzalez C, Pople JA (2004) Gaussian 03 (Revision E.01). Gaussian, Inc, Wallingford
- Wagener M, Sadowsky J, Gasteiger J (1995) Autocorrelation of molecular surface properties for modeling corticosteroid binding globulin and cytosolic ah receptor activity by neural networks. *J Am Chem Soc* 117:7769–7775

32. Yang Y, Zhang WJ, Gao XM (2006) *Int J Quantum Chem* 106:1199–1207
33. Klymchenko AS, Demchenko AP (2002) *J Am Chem Soc* 124:12372–12379
34. Hennesy J, Testa AC (1972) *J Phys Chem* 76:3362–3365
35. Swaminathan M, Dogra SK (1983) An unusual behavior in the excited state proton transfer of 9,10-phenanthroimidazole. *Perkin Trans 2*:1641–1644
36. Becke AD (1993) Density-functional thermochemistry. III. The role of exact exchange. *J Chem Phys* 98:5648–5652
37. Kakker R, Katoch V (2002) Theoretical study of the excited state intramolecular proton transfer in barbituric acid. *THEOCHEM* 578:169–175
38. Paul BK, Mahanta S, Singh RB, Guchhait N (2010) A DFT based theoretical study on the photophysics of 4-hydroxyacridine: single-water-mediated excited state proton transfer. *J Phys Chem A* 114:2618–2627
39. Wu K-C, Ku P-J, Lin C-S, Shih H-T, Wu F-I, Huang M-J, Lin J-J, Chen I-C, Cheng C-H (2008) The photophysical properties of dipyrnylbenzenes and their application as exceedingly efficient blue emitters for electroluminescent devices. *Adv Funct Mater* 18:67–75